*Journal of Ceramic Processing Research. Vol. 18, No. 7, pp. 526~530 (2017)*

J O U R N A L O F
**Ceramic Processing Research**

# Effect of hydrothermal temperature on microstructure and optical properties of $ZnIn_2S_4$ microspheres and their photocatalytic degradation of methylene blue

**Watcharapong Pudkon[a,b], Titipun Thongtem[a], Somchai Thongtem[c], Sila Kittiwachana[a,d] and Sulawan Kaowphong[a,d,*]**

[a]*Department of Chemistry, Faculty of Science, Chiang Mai University, Chiang Mai 50200, Thailand*
[b]*Graduate School, Chiang Mai University, Chiang Mai 50200, Thailand*
[c]*Department of Physics and Materials Science, Faculty of Science, Chiang Mai University, Chiang Mai 50200, Thailand*
[d]*Center of Excellence in Materials Science and Technology, Chiang Mai University, Chiang Mai 50200, Thailand*

**$ZnIn_2S_4$ microspheres were synthesized via a hydrothermal method using zinc chloride ($ZnCl_2$), indium chloride tetrahydrate ($InCl_3 \cdot 4H_2O$) and L-cysteine ($C_3H_7NO_2S$). The effect of hydrothermal temperatures (160 °C, 200 °C and 240 °C) on the crystallinity, morphology and optical properties of the synthesized powders was investigated. The synthesized products were characterized by X-ray diffraction (XRD), Fourier transform infrared spectroscopy (FT-IR), field emission scanning electron microscope (FE-SEM) and transmission electron microscope (TEM). The results showed that the synthesized powders were pure $ZnIn_2S_4$ with a hexagonal structure. The $ZnIn_2S_4$ powders were microspheres with diameters of 8.3-9.5 μm, constructed from several nanosheets. These nanosheets interconnected with each other, forming a pore structure. With increasing hydrothermal temperature, the nanosheets increased in thickness and the width of the pores between the nanosheets expanded. The $ZnIn_2S_4$ powder synthesized at 240 °C exhibited stronger UV-Vis absorption and photoluminescence (PL) intensities than the other samples. The photocatalytic activity of the $ZnIn_2S_4$ photocatalyst was investigated by photodegradation of methylene blue under blue light irradiation; 97% of the methylene blue degraded within 210 min. Photostability of the $ZnIn_2S_4$ photocatalyst was also investigated.**

**Key words: Zinc indium sulfide, Photocatalysts, Hydrothermal, Optical properties.**

## Introduction

Wastewater containing dyes released from textile and paper industries is a serious environmental problem. Decontaminating polluted water by semiconductor photocatalysis has attracted considerable attention for its efficiency and potential cost effectiveness [1]. Zinc indium sulfide ($ZnIn_2S_4$), a ternary sulfide semiconductor with a direct band gap of 2.3 eV [2], has been considered as a good candidate for visible-light-driven photocatalytic applications such as $H_2$ evolution from pure water and degradation of organic dyes [3-5].

Hydrothermal synthesis is widely applied to prepare various semiconductor nanomaterials. In this method, chemical reactions are carried out in an autoclave in the presence of an aqueous solvent under autogenous pressure and elevated temperature; this allows for greater solubility of solids for the reaction process, and the materials can be synthesized at lower temperatures compared to a solid-state reaction method [6]. The desired physicochemical properties of the materials can be controlled by adjusting synthesis parameters, such as type of precursors [7], type of solvents [8, 9], additives [10], and reaction times [11, 12].

Temperature is one of the most important parameters that affects nucleation and particle growth of materials [12-15]. This research synthesized $ZnIn_2S_4$ microspheres by a hydrothermal method. We expect that by altering the hydrothermal temperature we can tailor the purity, crystallinity, size, and microstructures of the synthesized $ZnIn_2S_4$ microspheres. We investigated the optical properties of the synthesized materials, as well as their photocatalytic activity in treating wastewater treatment by evaluating the degradation of methylene blue under blue LED lamp as a light source.

## Experimental Procedure

### Synthesis of $ZnIn_2S_4$

$ZnCl_2$ (2.5 mmol), $InCl_3 \cdot 4H_2O$ (5.0 mmol), and L–cysteine (10.0 mmol) were dissolved in 50 mL of de-ionized water. After constant stirring for 15 min, the mixture was transferred into a Teflon-lined stainless steel autoclave with a capacity of 75 mL. The autoclave was sealed and heated at 160, 200 and 240 °C for 48 hrs and naturally cooled to room temperature. Finally, the powders were separated from the mother liquor by filtering, then washed several times with de-ionized water and dried at 80 °C for 24 hrs.

*Corresponding author:
Tel : +66-53-943341
Fax: +66-53-892277
E-mail: sulawank@gmail.com

## Characterization

The purity, crystallinity, and crystal structure of the synthesized powders were characterized by XRD (Rigaku MiniFlex II) with a Cu*K*α radiation (1.5406 Å). Residual organic molecules were investigated by FT-IR (Bruker TENSOR27) using the KBr pellet technique. Particle size and morphology of the powders were determined by FE-SEM (Jeol JSM-6335F), operated at 15 kV of accelerating voltage and TEM (Jeol JEM-2010), operating at 200 kV. UV-Vis absorption spectra were recorded by UV-Vis spectrophotometer (Lamda25 PerkinElmer). Photoluminescence (PL) spectra of the powders were measured using a photoluminescence spectrometer (Avantes Avaspec-2048TEC-USB2) with an excitation wavelength of 345 nm.

## Photocatalytic activity and stability testing

$ZnIn_2S_4$ powder (100 mg) was dispersed in an aqueous solution of methylene blue (200 mL, 10 $mgL^{-1}$). Prior to irradiation, the suspension was magnetically stirred in a dark condition for 30 min to establish the adsorption-desorption equilibrium on the $ZnIn_2S_4$ surfaces. The reaction system was then irradiated under ten 5 W LED lamps (465 nm) as the light source for 0-210 min. 5 mL of the sample was taken from the reaction solution every 15 min and the degraded methylene blue solutions were determined by UV-Vis spectrophotometer at 645 nm. Methylene blue photolysis (without catalyst) was also performed under the same experimental conditions. The decolorization efficiency (%DE) was calculated using the following equation:

$$\%DE = \frac{(C_0 - C)}{C_0} \times 100 \quad (1)$$

where $C_0$ and $C$ are the concentrations of methylene blue before and after the light irradiation, respectively.

To evaluate the photostability of the $ZnIn_2S_4$ photocatalyst, after the first run, the photocatalyst was separated by centrifuged from the suspension, washed with water, and dried at 80 ºC. Then, the recovered photocatalyst was reused for the next run of the photocatalytic degradation reaction under the same conditions.

## Results and Discussion

Fig. 1(a) shows the FT-IR spectra of L-cysteine and the powders synthesized at different hydrothermal temperatures. No absorption peaks originating from L-cysteine were detected in the FT-IR spectra of the synthesized powders, indicating that the L-cysteine molecules were completely decomposed at given hydrothermal temperatures. The XRD pattern of the powders synthesized at different hydrothermal temperatures is shown in Fig. 1(b). All of the diffraction peaks can be indexed as a hexagonal $ZnIn_2S_4$ structure, according to ICDD database no. 01-072-0730. No characteristic peaks arising from possible impurities such as ZnS, $In_2S_3$ or oxides were observed, indicating that high purity $ZnIn_2S_4$ crystals with hexagonal structure is formed. The diffraction peaks of the $ZnIn_2S_4$ powders gradually strengthened and narrowed with increasing hydrothermal temperature, suggesting an increase in crystallinity and crystallite size. The crystallite sizes of the $ZnIn_2S_4$ particles can be calculated from the (110) diffraction peak by applying the Debye-Scherrer equation [16]:

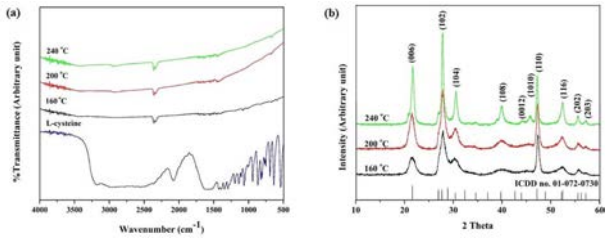


**Fig. 1.** (a) FT-IR spectra of the powders synthesized at different hydrothermal temperatures compared with FT-IR spectrum of L-cysteine and (b) XRD pattern of the powders synthesized at different hydrothermal temperatures.

**Table 1.** XRD diffraction angle ($2\theta$), FWHM, and calculated crystallite size ($D$) of the $ZnIn_2S_4$ particles synthesized at different hydrothermal temperatures.

| Temperature/ °C | $2\theta$/ deg | FWHM/ radian | $D$ (110)/ nm |
|---|---|---|---|
| 160 | 47.3343 | 0.006185 | 24.48 |
| 200 | 47.2305 | 0.004811 | 31.46 |
| 240 | 47.2279 | 0.002749 | 55.06 |

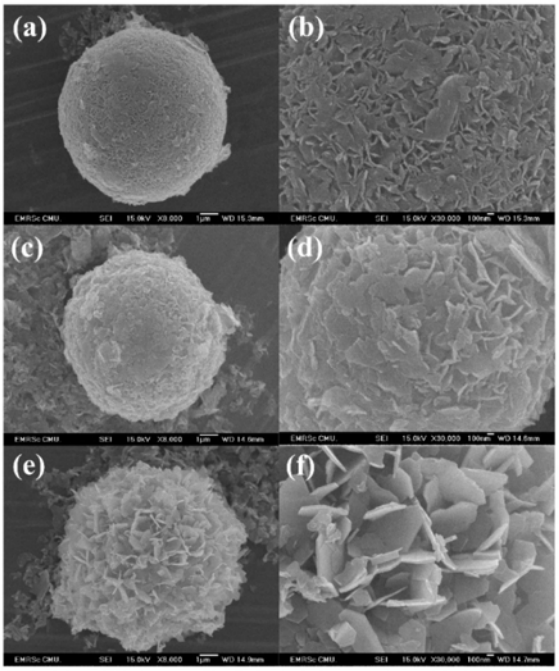


**Fig. 2.** FE-SEM images of the $ZnIn_2S_4$ powders synthesized at ((a) and (b)) 160 ºC, ((c) and (d)) 200 ºC, and ((e) and (f)) 240 ºC.

$$D = \frac{0.9\lambda}{B\cos\theta} \quad (2)$$

where $D$ is the crystallite size in nanometers, $\lambda$ is the wavelength of Cu$K_\alpha$, $B$ is the full width at half-maximum (FWHM) in radian and $\theta$ is the half-diffraction angle in degrees. The XRD diffraction angle, FWHM, and calculated crystallite size of the $ZnIn_2S_4$ powders synthesized at different hydrothermal temperatures are summarized in Table 1. The results showed that the FWHM of the diffraction peaks tended to decrease with increasing in hydrothermal temperature, corresponding to the increasing crystallite sizes. This suggests that higher hydrothermal temperatures are beneficial to the growth of $ZnIn_2S_4$ crystals.

Fig. 2 shows the FE-SEM images of the $ZnIn_2S_4$ powders synthesized at different hydrothermal temperatures. The synthesized $ZnIn_2S_4$ powders were composed of microspheres with diameters in the range of 8.3-9.5 μm, and pores can be observed on the surface of the microspheres (Figs. 2(a), 2(c), and 2(e)). The high-magnification FE-SEM images (Figs. 2(b), 2(d), and 2(f)) showed that the $ZnIn_2S_4$ microspheres were composed of many randomly grown nanosheets, with average thickness in the range of 20-80 nm. These nanosheets interconnected with each other, forming a pore structure. With increasing of the hydrothermal temperature, the nanosheets increased in thickness, while the diameter of the microspheres did not change significantly. This could relate to the Ostwald ripening process, in which larger sheets grow at the expense of smaller sheets. In addition, the width of the pores between the nanosheets further expanded with increasing hydrothermal temperature, from 150 to 300 to 700 nm for the powders synthesized at 160, 200, and 240 °C, respectively. Well-defined flower-like microspheres with large and deep pores were observed on the surface of the $ZnIn_2S_4$ microspheres in the powder synthesized at 240 °C. This is essential to decreasing the interface contact resistance between the surface of $ZnIn_2S_4$ and dye molecules [17]. The growth mechanism of the $ZnIn_2S_4$ could be attributed to the formation of flower-like $ZnIn_2S_4$ microspheres as reported by Chen et al. [4].

The $ZnIn_2S_4$ powder synthesized at 240 °C was selected for the TEM investigation to clearly reveal the microstructure of the $ZnIn_2S_4$ microspheres. The $ZnIn_2S_4$ microspheres were composed of numerous nanosheets with thickness of about 80 nm on the surface of the $ZnIn_2S_4$ microspheres (Fig. 3(a)). The selected area electron diffraction (SAED) pattern of the $ZnIn_2S_4$ powder (Fig. 3(b)) showed bright concentric rings corresponding to (104), (101), (110) and (202) diffraction planes, confirming that the synthesized $ZnIn_2S_4$ microspheres were well-crystalline with a hexagonal structure, in accordance with the ICDD database.

Fig. 4(a) showed the UV-Vis absorption spectra of the $ZnIn_2S_4$ powders synthesized at different hydrothermal temperatures. The $ZnIn_2S_4$ powder synthesized at 240 °C

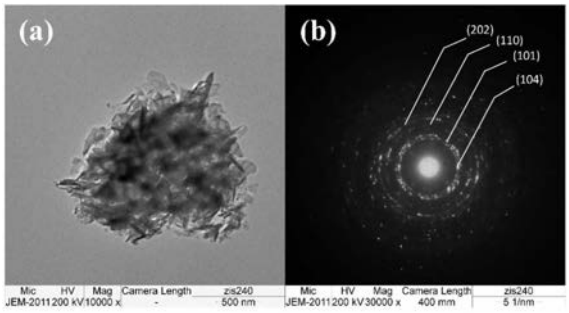


**Fig. 3.** (a) TEM image and (b) SAED pattern of the $ZnIn_2S_4$ powder synthesized at 240 °C.

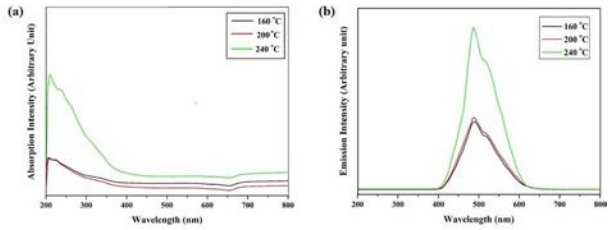


**Fig. 4.** (a) UV-Vis absorption spectra and (b) PL spectra of the $ZnIn_2S_4$ powders synthesized at different hydrothermal temperatures.

showed the strongest UV-Vis absorption intensity, probably because the abundance of large and deep pores on the surface of the well-defined flower-like $ZnIn_2S_4$ microspheres promoted efficient light harvesting and light multi-reflections of the incident light within their structures [18, 19]. The $ZnIn_2S_4$ with pore structure and strong UV-Vis absorption ability could exhibit a beneficial effect on photocatalytic activity. The PL spectra of the $ZnIn_2S_4$ powders synthesized at different hydrothermal temperatures are shown in Fig. 4(b). All of the PL spectra exhibited two emission peaks located at 480 and 520 nm under excitation wavelength at 345 nm. The $ZnIn_2S_4$ powder synthesized at 240 °C exhibited the strongest PL intensity. This can be explained by the large surface content of sulfur vacancies in the synthesized $ZnIn_2S_4$ particles [20]. In the excitonic PL process, the non-radiative transitions of photo-induced electrons from the conduction band bottom to different sub-bands (or surface states) occur first, and subsequent radiative transition from the sub-band to the valence band top follow [20]. Surface vacancies and defects in the materials cause the excitonic PL signal [20, 21]. Sulfur vacancies can bind photo-induced electrons to form excitions, as a result, PL signal could easily occur [20].

In the hexagonal $ZnIn_2S_4$ crystal structure, the atoms are stacked in a S-Zn-S-In-S-In-S sequence along the *c*-axis, and the negative S ions are exposed on the surface of the {0001} facets [17, 22]. The (0001) negative-charge S plane preferentially adsorbs cationic dyes [23]. Based on our experimental results and some previous reports [17-18, 22, 23], the photocatalytic activity of the $ZnIn_2S_4$ synthesized at 240 °C was

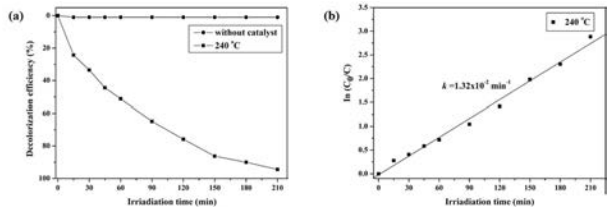


**Fig. 5.** (a) Decolorization efficiency of methylene blue and (b) Pseudo-first order kinetic of the $ZnIn_2S_4$ photocatalyst.

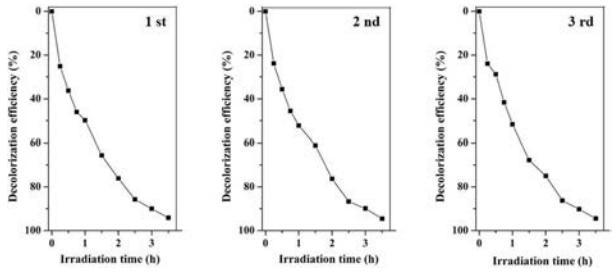


**Fig. 6.** Stability study of photocatalytic activity of photodegradation of methylene blue of the $ZnIn_2S_4$ photocatalyst.

expected to be better than the other samples, so chosen to further investigate photocatalytic activity. Photocatalytic activity was tested by photodegrading of methylene blue. Fig. 5(a) shows the %DE of methylene blue by the $ZnIn_2S_4$ photocatalyst synthesized at 240 °C under blue light irradiation. The photolysis test showed no obvious change in the concentration of methylene blue, illustrating that the self-degradation of methylene blue remained unchanged and was negligible under blue light irradiation. The $ZnIn_2S_4$ photocatalyst decolorized methylene blue with an efficiency of 97% after 210 min. Fig. 5(b) presents the photocatalytic reaction kinetic of the degradation of methylene blue; it shows a good correlation to pseudo-first-order reaction kinetic. The determined reaction rate constant ($k$) for the methylene blue degradation was $1.32 \times 10^{-2}$ $min^{-1}$.

To evaluate the photocatalytic stability of the $ZnIn_2S_4$ photocatalyst, we repeated the photocatalytic degradation of methylene blue experiments under the same conditions as shown in Fig. 6. No significant loss in photocatalytic degradation of methylene blue was observed during three test runs. This suggested that the $ZnIn_2S_4$ photocatalyst maintained its high photocatalytic performance for the photocatalytic degradation of methylene blue.

## Conclusions

$ZnIn_2S_4$ microspheres were synthesized by hydrothermal method. Hydrothermal temperature influenced the crystallinity, morphology, and optical properties of the synthesized $ZnIn_2S_4$ powders. At a hydrothermal temperature of 240 °C, well-defined flower-like $ZnIn_2S_4$ microspheres with highest crystallinity were formed with large and deep pores on their surfaces, providing the strongest UV-Vis absorption intensity. The $ZnIn_2S_4$ photocatalyst degraded 97% of methylene blue within 210 min, and the photocatalyst exhibited good stability over three test runs.

## Acknowledgments

This research was financially supported by the Thailand Research Fund (TRF) (Grant number MRG6080270), the Center of Excellence (CoE) in Materials Science and Technology, and the Chiang Mai University (CMU) Junior Research Fellowship Program. Watcharapong Pudkon would like to thank the Science Achievement Scholarship of Thailand and the Graduate School, Chiang Mai University.

## References

1. A.D. Paola, E. García-López, G. Marcì, and L. Palmisano, J. Hazard. Mater. 211-212 (2012) 3-29.
2. K.W. Cheng, C.M. Huang, Y.C. Yu, C.T. Li, C.K. Shu, and W. L. Liu, Sol. Energy Mater. Sol. Cells 95 (2011) 1940-1948.
3. S. Peng, M. Dan, F. Guo, H. Wang, and Y. Li, Colloids Surf. A Physicochem. Eng. Asp. 504 (2016) 18-25.
4. Y.J. Chen, S.W. Hu, W.J. Liu, X.Y. Chen, L. Wu, X. Wang, P. Liu, and Z. Li, Dalton Trans. 40 (2011) 2607-2613.
5. S.H. Shen, P.H. Guo, L. Zhao, Y.C. Du, and L.J. Guo, J. Solid State Chem. 184 (2011) 2250-2256.
6. K. Byrappa and T. Adschiri, Prog. Cryst. Growth Charact. Mater. 53 (2007) 117-166.
7. B.S. Kwak, B. Choi, M. Ji, S. Park, and M. Kang, J. Ind. Eng. Chem. 18 (2012) 11-15.
8. L. Su, X. Ye, S. Meng, X. Fu, and S. Chen, Appl. Surf. Sci. 384 (2016) 161-174.
9. W. Pudkon, S. Kittiwachana, T. Thongtem, S. Thongtem, and S. Kaowphong, Sci. Adv. Mater. 8 (2016) 138-143.
10. S. Shen, L. Zhao, and L. Guo, Mater. Res. Bull. 44 (2009) 100-105.
11. F. Fang, L. Chen, Y.B. Chen, and L.M. Wu, J. Phys. Chem. C 114 (2010) 2393-2397.
12. J. Yu, G. Wang, B. Cheng, and M. Zhou, Appl. Catal., B 69 (2007) 171-180.
13. D. Ke, T. Peng, L. Ma, P. Cai, and K. Dai, Inorg. Chem. 48 (2009) 4685-4691.
14. R. Huang, Y. Shen, L. Zhao, and M. Yan, Adv. Powder Technol. 23 (2012) 211–214.
15. M.A. Ballem, J.M. Cordoba, and M. Oden, Microporous Mesoporous Mater. 129 (2010) 106-111.
16. C. Suryanarayana and M.G. Norton, X–ray Diffraction: A practical approach, Plenum Press, New York, (1998) 207-221.
17. X. Hu, J.C. Yu, J. Gong, and Q. Li, Cryst. Growth Des. 7 (2007) 2444-2448.
18. X. Yu, J. Yu, B. Cheng, and M. Jaroniec, J. Phys. Chem. C 113 (2009) 17527-17535.
19. Y. Huo, J. Zhang, M. Miao, and Y. Jin, Appl. Catal. B 111–112 (2012) 334-341.
20. J. Liqiang, Q. Yichun, W. Baiqi, L. Shudan, J. Baojiang, Y. Libin, F. Wei, F. Honggang, and S. Jiazhong, Sol. Energy Mater. Sol. Cells 90 (2006) 1773-1787.
21. P. Dong, G. Hou, C. Liu, X. Zhang, H. Tian, F. Xu, X. Xi, and R. Shao, Materials 9 (2016) 968 (1-17).

22. C. Tan, G. Zhu, M. Hojamberdiev, K.S. Lokesh, X. Luo, L. Jin, J. Zhou, and P. Liu, J. Hazard. Mater. 278 (2014) 572-583.

23. Y. Chen, R. Huang, D. Chen, Y. Wang, W. Liu, X. Li, and Z. Li, Appl. Mater. Interface. 4 (2012) 2273-2279.